2015

Analyses of ionizing radiation effects in – vitro in peripheral blood 1 lymphocytes with Raman spectroscopy

Adrian Maguire
Technological University Dublin

Isabel Vegacarrascal
Technological University Dublin

Lisa White
Technological University Dublin, lisa.white2@mydit.ie

See next page for additional authors

Recommended Citation

Maguire, A., Vegacarrascal, I. & White, L. (2015). Analyses of ionizing radiation effects in – vitro in peripheral blood 1 lymphocytes with Raman spectroscopy. *Radiation Research*, vol. 183, no. 4, pp. 407-416. doi.org/10.1667/RR13891.1

Analyses of ionizing radiation effects in – vitro in peripheral blood lymphocytes with Raman spectroscopy

A. Maguire [1,3], I. Vegacarrascal [1], L. White [1,2], B. McClean[4], O. Howe [1,2], F.M. Lyng [1,3], A.D. Meade [1,3]

1. DIT Centre for Radiation and Environmental Science, Focas Research Institute, Camden Row, Dublin 8, Ireland
2. School of Biological Sciences, Dublin Institute of Technology, Kevin Street, Dublin 8, Ireland
3. School of Physics Dublin Institute of Technology, Kevin Street, Dublin 8, Ireland
4. Department of Medical Physics, St Luke's Hospital (SLROC), Highfield Road, Rathgar, Dublin 6, Ireland

Corresponding Author:
Aidan.Meade@dit.ie

Analyses of ionizing radiation effects in – vitro in peripheral blood lymphocytes with Raman spectroscopy

A. Maguire [1,3], I. Vegacarrascal [1], L. White [1,2], B. McClean[4], O. Howe [1,2], F.M. Lyng [1,3], A.D. Meade [1,3]

The use of Raman spectroscopy to measure the biochemical profile of cells and tissue in health and disease may be a possible solution to many diagnostic problems in the clinical setting. Although its application has been extensive in identifying changes in the biochemical profiles of cancerous cells and tissue, its application for analysing changes to the cellular environment by external factors such as ionizing radiation has been less extensive. In tandem with this, the biological impact of low doses of ionizing radiation remains poorly understood. Extensive studies have been performed on the radiobiological effects associated with doses above 0.1Gy, and are well characterized, but current studies of low dose exposure to ionizing radiation reveal complex and highly variable responses to low dose exposures.

The current study demonstrates, for the first time, the capability of Raman spectroscopy to detect radiation-induced damage responses in isolated lymphocytes from donors irradiated to doses of 0.05 Gy and 0.5 Gy. Lymphocytes were isolated from peripheral blood in a cohort of volunteers, were cultured ex-vivo, and then irradiated. Within 1 hour after irradiation spectral effects were observed with Raman micro-spectroscopy and Principal Component Analysis - Linear Discriminant Analysis (PCA-LDA) at both doses relative to the sham-irradiated 0Gy control. Cellular DNA damage was confirmed using parallel γ-H2AX fluorescence measurements on the extractred lymphocytes per donor and per dose. DNA damage measurements exhibited inter-individual variability between both donors and dose, which matched that seen in the spectral variability in the lymphocyte cohort. Further evidence of links between spectral features and DNA damage were also observed, and may potentially allow non-invasive insight into the DNA remodeling after exposure to ionizing radiation.

1. Introduction

The mechanisms affecting high dose cell survival (at doses above ~0.1Gy) have been studied extensively and are relatively well understood for a wide range of cell lines *(1)*. The mechanisms affecting low dose cell survival (at doses below ~0.1Gy) phenomena, such as low dose hyper-radiosensitivity and increased radioresistance are yet to be fully understood *(2)*. Studies have shown that a region of hyper radiosensitivity (HRS) in the dose region from 0-0.3Gy, followed by a region of increased radioresistance (IRR) in the region 0.3-0.6Gy *(2)*, exists in many but not all cell types *(3)*, including peripheral blood lymphocytes *(4)*.

Some suggest that this transition period is due to the activation of DNA repair systems such as the activation of the ataxia telangiectaisa-mutated (ATM) gene for the recruitment of further repair proteins such as the MRN complex (RAD50, MRE11 and NBS1) , which is responsible for the activation of down-stream pathways *(5)*. While there are a myriad of lesion types that can occur following ionizing radiation, double strand breaks (DSBs) can be the most lethal and mutagenic if not repaired properly *(6)*. Defects in repair pathways of DSBs can result in severe responses to radiotherapy or mis-diagnosis of exposure in dosimetry estimates. Histone H2AX is a molecule that is recruited to the site of DSBs. ATM phosphorylates H2AX to form γ-H2AX which is then used to recruit further repair molecules to the site of DSBs *(7)*. If the ATM gene is defective then this process cannot occur through the action of ATM and other less proficient pathways may be activated. The measurement of phosphorylation of H2AX to γ-H2AX has been used as a method of assessing DNA damage and repair. The use of the γ-H2AX assay has been demonstrated as a technique that may be used for retrospective personal biodosimetry, however considerable inter-individual variation in baseline levels of γ-H2AX fluorescence is problematic with this assay *(9)*. Other approaches may therefore be necessary to allow retrospective dosimetry using direct biological measurements on exposed individuals.

Vibrational spectroscopy, both FTIR and Raman spectroscopy, has become a useful tool for providing a complete biochemical profile of cellular contents, including nucleic acid, proteins,

lipids and fatty acids. Both FTIR and Raman spectroscopy have been shown to be useful for the diagnosis of diseased and healthy cells based on their biochemical profiles *(10–12)* and while extensive efforts have been made to standardize these techniques Raman spectroscopy has yet to reach the clinic as a method of diagnosis. Although much emphasis has been focused on disease diagnosis, Raman spectroscopy has been shown to have potential in the analysis of radiobiological effects at high ionizing radiation doses in prostate tumor cell lines *(13)*. The spectral response following high doses of ionizing radiation in *(13)* showed changes in spectral intensities of the bands associated with the O-P-O vibration of the DNA back bone at ~810cm^{-1}, nucleic acid bases (U,T,C,G and A, from DNA and RNA) at 784, 1486 and 1577cm^{-1}, and several bands associated with vibrations from lipids and proteins (C-C,C-N vibrations at 936 and 1127cm^{-1}) that allowed for disctrimination between sham irradiated and irradiated cells at 24 hours following ionizing radiation. In addition, FTIR spectra of irradiated human skin cells have demonstrated dose-dependent spectral changes that have been used for biodosimetry at both low (<0.1Gy) and high (>0.1Gy) doses *(14)*. In this study the authors show that difference in absorbance spectra occur at bands associated with various vibrations arising from DNA, RNA and carbohydrates (overlapping vibrations from C-O at 1200 and 1030cm^{-1} and O-H vibrations at 1290 and 1030) along with other characteristic vibrations from nucleic acids (U at 996cm^{-1} and PO_4^- at 965cm^{-1}).

The present study demonstrates for the first time the ability of Raman spectroscopy to detect low dose ionizing radiation effects in lymphocytes derived from a cohort of healthy donors. Discrimination of radiation damage through the use of spectral profile changes is shown to be possible at γ-radiation doses of 0.05Gy and 0.5Gy, which straddle the inflection in the cell survival curve in the low dose region. Changes in spectral profiles of individuals were found to be highly variable, making it difficult to create a model capable of predicting individual response to low dose ionizing radiation for its use in low dose dosimetry.

2. Materials and methods

Ethical approval

Ethics approval was awarded by the Dublin Institute of Technology ethics committee (2012) for the collection of blood donations from volunteers at the Institute for the purposes of this study. Volunteers consisted of both male and female donors within the age range of 21 to 56, and contained both smokers and non-smokers.

Peripheral blood lymphocyte isolation

A total of 20ml of fresh whole blood was drawn into lithium heparin tubes after obtaining informed consent from each of the donors. Peripheral blood mononuclear cells (PBMC) were isolated within 4h of sample collection. A total of 6 ml of Dulbecco's modified phosphate buffered saline (DPBS) (Sigma) was added to 6 ml of heparinised blood, mixed by gentle inversion and overlaid over 15 ml of Histopaque. Samples were then centrifuged at 400g for 30 min at room temperature. The PBMC layer was removed and washed three times. Finally, cells were centrifuged at 250g for 5 minutes at room temperature. The cell pellet was then resuspended in 3 ml of full media (RPMI+12.5 %(v/v) FBS + 2 mML-glutamine (Sigma)) supplemented with 2.5% (v/v) phytohaemagglutinin (PAA Laboratories). One ml of cell suspension was transferred to a T25 flask containing 4ml of full media. A total of 3 flasks were prepared for each donor and they were incubated for 72 hours at 37°C, 5% CO_2 to allow separation of lymphocytes and monocytes by plastic adherence.

Cell Irradiation and slide preparation

A total of 5ml of cell suspension was placed in T25 flasks for irradiation. The flasks were either sham irradiated (0Gy) or irradiated (0.05Gy and 0.5Gy) 17 hours after plating using a cobalt 60 gamma ray teletherapy source at St. Luke's hospital, Dublin. The dose rate was approximately 1.5 Gy/min during these experiments and was determined from a decay corrected measurement of the in-beam axial dose at an 80cm source to chamber distance (measured using a secondary standard ionization chamber within a water equivalent phantom). The dose settings that were used and the actual dose delivered, with their respective uncertainties, were 0.05Gy (0.058Gy ± 17%) and 0.5Gy (0.511Gy ± 2%). The

actual dose that was delivered at the time of irradiation was determined from the axial dose, corrected for scatter and grid factors, the additional time that the sample was exposed to radiation ((with an accuracy of ± 0.005 min) during the extension and recession of the source from the within the cobalt unit), and source to sample distance (191.5cm for 0.05Gy and 100cm for 0.5Gy). The samples were then placed in an incubator at 37°C for 60 mins at which time, cells were fixed using 2% paraformaldehyde in phosphate-buffered saline. From the suspension, 40 µl was drop cast onto calcium fluoride (CaF_2) slides. The slides were then washed in deionised H_2O and the samples were allowed to dry for Raman spectroscopic measurements.

Raman Spectroscopy

Raman spectroscopy was performed using a Horiba Jobin Yvon Labram HR800 UV system, equipped with a 660nm solid-state diode laser delivering 100mW of power to the sample. Spectra were acquired for each of 20 different donors over a period of 6 months. All samples (sham irradiated cells (0Gy) and irradiated samples (0.05Gy and 0.5Gy) from each individual were recorded on the same day, together with a spectrum of 1,4-Bis (2-methylstyryl) benzene and NIST SRM 2245 for calibration purposes. Multiple calibration spectra were recorded before recording a sequential group of cellular spectra. Spectra were recorded from 30-40 cells per dose and time point and from each of the independent donors. The cells were ~8-12µm in size and each spectrum was recorded from individual cells using a 4x4µm raster scan of the cell including both signal from its nucleus and cytoplasm. Spectra were recorded with a 20 second integration time and averaged across three integrations per spectrum. Spectra were recorded using a diffraction grating ruled with 300 lines/mm giving a spectral resolution of ~2.1cm^{-1}. The confocal hole was set to 150µm with the grating centered at 1350cm^{-1}. All spectra were recorded within two weeks of slide preparation. Slides were stored in a desiccator until measurement.

Raman spectral post processing

All post processing was performed using Matlab version 7.9.0 (R2009b; Mathworks, USA) using the PLS-Toolbox version 6.51 (Eigenvector Research Inc.) and in-house algorithms. The spectra were

wavenumber aligned using the calibration spectrum of 1, 4-Bis (2-methylstyryl) benzene through the fitting of a polynomial to the relative positions of peaks in the calibration spectrum versus those in a common reference spectrum of the substance. This results in a spectral misalignment of <0.1 cm^{-1} through day-to-day variation. Spectral intensity calibration was also performed using a reference spectrum of standard reference material SRM2245 (NIST). Baseline correction was performed using a nodal point baseline correction using the minimum amount of points possible to ensure minimal alteration of the spectra. Spectra were then lightly smoothed using a Savitsky Golay filter (5th order, 15 point window). Substrate contributions from the CaF_2 slide were also subtracted from the cellular spectra. All spectra were subsequently vector normalised before analysis.

Principal component analysis-Linear discriminant analysis and statistical analysis

Multivariate data classification approaches including Principal Component Analysis (PCA) with Linear Discriminant Analysis (LDA) have been used to identify features that can classify spectra in an unsupervised manner *(10,15).* Cellular Raman spectra consist of many overlapping regions from different constituents. PCA removes this redundancy while LDA attempts to discriminate between conditions using the previously determined principal components. In this study PCA-LDA is used to discriminate between sham irradiated and irradiated donor lymphocytes. All classifications in this study were performed using a Leave-One-Out-Cross validation (LOOCV) approach and confusion matrices, sensitivities and specificities were calculated on the basis of LOOCV.

Statistical testing of each wavenumber was performed across the spectrum, to identify regions of the spectrum that the irradiated spectra varied significantly from the sham irradiated spectra. Significance testing was performed using a two tailed t-test independently on each wavenumber. Each irradiated samples wavenumber was found to be significantly different from the sham if the significance level was found to be $p<0.05$.

γ-H2AX assay

Cells were fixed at 1 hour after irradiation and frozen at -20ºC. They were later permeabilised in 200-1000µl of 0.25% (v/v) Triton X-100 in PBS and incubated for 5 minutes at room temperature. Permeabilisation solution was then removed and the cells were resuspended in 200µl of blocking solution (PBS containing 2% (w/v) BSA) and incubated for 30 minutes at room temperature. Blocking solution was removed and the cells were resuspended in 150µl of primary antibody solution (Anti-phospho-histone H2AX, diluted 1:500 in blocking solution, Millipore) and incubated for a further 2 hours at room temperature. Washing was performed three times in 500µl of PBS and 150µl of secondary antibody solution (Alexa Fluor 488, diluted 1:200 in blocking solution, Invitrogen) was then added. The cells were incubated at room temperature for 1 hour in the dark and washing was performed in 500µl PBS three times. Fluorescence was analysed using a BD Accuri C6 flow cytometer. The mean fluorescence signal intensity due to green Alexa Fluor 488 dye was measured. A minimum of 10,000 events per sample were recorded, debris and cell aggregates were removed from the analysis using forward (FSC) and side scatter (SSC) characteristics. Significance testing was performed between sham irradiated and irradiated γ-H2AX measurements using a two tailed paired t-test.

3. Results

Raman spectroscopic analysis of sham irradiated and irradiated donor lymphocytes.

Figure 1 A shows the mean spectra from sham irradiated (0Gy) lymphocytes from 20 donors along with the pure spectra of DNA, RNA, phosphatidyl-inositol and actin. The spectral profiles of donor lymphocytes in this study are consistent with that observed in previous studies by *(16–19)*, with bands observed at 770-790 cm^{-1} arising from vibrations associated with the DNA double helix, 1000-1003 cm^{-1} occurring as a result of the vibrations of phenylalanine *(20)* and bands occurring in the regions

1250-1350, 1400-1450 and 1500-1700 cm^{-1} (Amide I,II and III bands) associated with proteins, lipids and nucleic acids *(21,22)*. The dotted dashed lines in the plot are to highlight typical spectral bands associated with biological species and band assignments are provided in table 1. Figure 1 B (top) shows the difference spectrum of sham irradiated and irradiated (0.05Gy) cells and the difference spectrum of sham irradiated and irradiated (0.5Gy) (bottom) cells fixed at 1 hour following ionizing radiation. Samples were fixed at one hour following ionizing radiation in order to correlate the initial DNA damage sensing measured by the change in Raman spectral profiles, to the DNA damage sensing measured by the γ-H2AX assay. Analysis of later time points would result in measurement of residual damage rather than initial DNA damage sensing (measured by γ-H2AX), where Raman spectroscopy may also measure changes in spectral profiles due to pathways downstream of initial sensing, such as cell cycle arrest, senescence and apoptosis. These cellular processes will result in changes in spectral profiles due to the up or down regulation of repair proteins and proteins associated with the other DNA damage responses in addition to the changes in spectral profiles due to the initial DNA damage response. The spectra of pure DNA and actin are plotted above and below the difference spectrum to highlight some of the origins of the change in spectral profiles of donor lymphocytes following ionizing radiation. The lightly shaded regions of Figure 1 B represent regions of the spectrum where irradiated samples had significantly higher intensities than that of the sham. The darker shaded regions represent regions of the spectrum where irradiated samples had significantly lower intensities than that of the sham. A similar change is observed in both doses with the exception of the band at 1650cm^{-1} in the Amide I region, which is associated with C=C stretching in protein and lipid *(38)*. Increases in the regions 610-620 cm^{-1} (associated with C-C twisting of aromatic ring structure *(20,23)*), 635-640 cm^{-1} (C-S stretching and C-C twisting of proteins *(20)*), 715-825 cm^{-1} (C-N membrane of phospholipids and phosphatidylcholine, A, T, U and C ring breathing and O-P-O DNA backbone stretching *(22,24–27)*), 845-850 cm^{-1} (Monosacchrides, polysaccrides and glucose *(22,28)*), 927-955 cm^{-1} (C-C stretching of amino acids proline and valine *(29)*), 1320-1340 cm^{-1} (G (DNA/RNA) and CH deformation *(27)*), 1565-1650 cm^{-1} (G and A nucleic acids and C=C bending *(29,30)*) and 1750-1800 cm^{-1} (C=O and C=C in lipids and fatty acids *(24,31)*)

were observed following ionizing radiation. Decreases in the regions 675-700 cm^{-1} (Ring breathing of DNA base G *(20)*), 1005-1020 cm^{-1} ((significantly less after 0.5Gy only) Phenylalanine and stretching of C-O of ribose *(27,32)*), 1085-1090 cm^{-1} (C-C vibration of acyl backbone in lipids and PO_2 stretching *(21,24,33)*), 1100-1125 cm^{-1} (Amide III *(21)*), 1255-1275 cm^{-1} (A, T, C and G nucleic acids, Amide III *(20,26,34,35)*), 1420-1425 cm^{-1} (G, A of nucleic acids and CH deformation *(27)*) and 1450-1525 cm^{-1} (CH_2 bending, C=N stretching of lipids *(36,37)*) were observed following ionizing radiation. Although there is a change in the mean of the intensities of these bands, the distributions overlap considerably across the cohort of donors.

Figure 2 A shows the difference spectra of control versus 0.05Gy in a total of 5 donors. In all cases there is a change in spectral profiles in the region 700-830cm^{-1} associated with nucleic acids and the phosphate backbone of DNA, the region 1070-1115cm^{-1} associated with C-C stretching of lipids and fatty acids, the band at 1094 cm^{-1} associated with the O-P-O stretching vibration of the DNA backbone, the region from 1550-1600 cm^{-1} associated with amide II band, tryptophan, guanine and adenine, and the region 1640-1730 cm^{-1} associated with the amide I, proteins, lipids and fatty acids. Although the variation consistently occurs in these regions the changes in spectral profile after 0.05Gy irradiation are inconsistent, with some donors having increases in band intensities in these regions and others having decreases in band intensities. Aside from these regions there is a large variation in the changes in spectral profiles following ionizing radiation throughout the rest of the spectrum, with large variation occurring in the region 1150-1520 cm^{-1} which is associated with nucleic acids, proteins, lipids and fatty acids. Similar variation is observed in the spectral changes following 0.5Gy of ionizing radiation. Figure 2 B shows the difference spectra of 0.5Gy and 0Gy for a different 5 donors. Again variations are consistently observed in the regions 700-830cm^{-1}, 1070-1115cm^{-1} and 1550-1600 cm^{-1}, but the change in spectral profile in these regions is inconsistent from donor to donor. This matches that of the inter-individual variability in the baseline levels of γ-H2AX which are discussed under the *γ-H2AX fluorescence measurements* section.

Classification of donor cohort by dose.

PCA-LDA was performed on each donor's spectra independently and classifications were performed on control spectra against 0.05Gy spectra, control spectra against 0.5Gy spectra and 0.05Gy against 0.5Gy spectra. PCA-LDA was performed using three principal components which were selected to maximize the sensitivity and specificity of each classification and such that they explained ~80% of the total variance in the spectra. The performance of the classifiers was calculated using leave-one-out-cross-validation (LOOCV). Figure 3 A shows the scatter plot of the PCA-LDA classification of sham irradiated and irradiated cells (0.05Gy) spectra from a single donor (Donor number 5). Principal component loadings are not shown due to the large inter-individual variability in the spectral features associated with the classification, however in all instances the principal components for each individual showed a high correlation to that of their difference spectra shown in Figure 2. The Matthews correlation coefficient (MCC) of the classification in Figure 3 A, was 0.79 with a sensitivity of 0.81 and a specificity of 1. MCC is used here to give a weighted combination of sensitivity and specificity, a value of +1 results in a classifier that predicts all instances correctly, a value of 0 results in a classifier that has a 50% chance of classifying any instance correctly and a value of -1 indicates that the classifier classifies each instance incorrectly. Figure 3 B shows the scatter plot of the PCA-LDA classification of sham irradiated and irradiated cells (0.5Gy) from the same donor. The Mathews correlation coefficient of this classification was 0.93 with a sensitivity of 0.97 and a specificity of 0.97. In Figure 3 A the second principal component, which explains 22% of the total variance, is the principal component primarily responsible for the classification as the separation in the classes occurs along its axis. In Figure 3 the classification is due to a combination of principal components two and three mainly. The first principal component in both classifications was found to be almost identical and contributes very little to the performance of the classification (Principal component not shown). This principal component may arise from the variability in the spectra which arises from the inherent variability in the cell cycle distribution within the cell population, as the features in this component were found to be consistent with those observed by Matthews et al in *(40)*. In both studies positive peaks in the first principal component occurred at

~670cm^{-1} (Guanine and thymine), 719cm^{-1} (choline), 728cm^{-1} (Adenine), 1100cm^{-1} (Phosphate backbone of DNA/RNA), ~1245cm^{-1} (Amide III β), 1450-1480cm^{-1} (Adenine, Guanine), 1575cm^{-1} (Adenine, Guanine) and 1680cm^{-1}(Amide I β). Negative peaks were observed in the principal components of both studies at ~700cm^{-1} (cholesterol),~ 1130cm^{-1} (C-C from lipids and C-N from proteins) and 1440cm^{-1} (CH2 deformation).

PCA-LDA classification models were created for each donors sham irradiated and irradiated cells separately. A mean sensitivity and specificity of 0.88 (σ = 0.1) and 0.91 (σ = 0.07) respectively were obtained for classification of spectra from the 0.05Gy samples versus the sham irradiated samples. Similarly sensitivities and specificities of 0.92 (σ = 0.07) and 0.93 (σ = 0.07) respectively were seen in the classification of the 0.5Gy samples versus the sham. The sensitivities and specificities for each donor's classifications are listed in table 2, in order of decreasing values of sensitivity. Larger values of sensitivity and specificity indicate larger changes in spectral profiles between classification conditions (0Gy v 0.05Gy, 0Gy v 0.5Gy or 0.05Gy v 0.5Gy). The variation in the classification sensitivities and specificities at each dose point demonstrates the variability in the changes in spectral profile of lymphocytes from donor to donor after ionizing radiation, which matches that of the variability of the dose response in the γ-H2AX assay. The classification rates for each individual show clearly that Raman spectroscopy can detect changes in spectral profiles between sham irradiated and irradiated cells at doses as low as 0.05Gy.

PCA-LDA classification was also performed using a pooled set of all on all donor spectra simultaneously. Classification of sham irradiated versus 0.05Gy and sham irradiated versus 0.5Gy, using a set of latent variables explaining up to 90% of the total variance of the spectra, demonstrated that there was a spectral difference between sham irradiated and irradiated cells with a mean MCC of 0.32 and 0.41 across all donors. Classification accuracies were estimated using a leave-one-donor-out cross-validation for varying numbers of latent variables to optimize the classification rate. Optimisation was performed using the training (all spectra except those from a single held-back donor) and testing (held-back spectra from one donor) sets of control versus 0.5Gy spectra. Both

training and testing sets classification performance was assessed using MCC. The training set performed relatively well when 35 or more latent variables were used in the classification and resulted in an MCC>0.3, however no model performed well on the test set where no model achieved an MCC of greater than 0.05 (data not shown). This demonstrates that although Raman spectroscopy can detect changes in biochemical profiles of individual donors following ionizing radiation, classification of response in individuals using data learned from a cohort of donors is difficult as demonstrated by the optimization not achieving an MCC greater than 0.05.

γ-H2AX fluorescence measurements

Parallel reference measurements of DNA damage following ionizing radiation were obtained using the γ-H2AX assay. A large inter-individual variation in baseline levels of γ-H2AX fluorescence was observed. In this study a significant difference was observed in γ-H2AX fluorescence following ionizing radiation only when samples where normalized to their own control (two tailed paired t-test). Figure 4 A) shows the normalized γ-H2AX fluorescence with respect to dose. A dose response was observed following ionizing radiation and 0.05Gy was found to be significantly different from the control with a significance level of $p<0.05$, while 0.5Gy was found to be significantly different from the controls with a significance level of $p<0.01$. The variation in inter-individual response to ionizing radiation detected using γ-H2AX fluorescence is consistent with that of the variation observed in the classification of Raman spectral data. In some donors the γ-H2AX fluorescence increases more so than others following ionizing radiation; similarly the change in spectral information following ionizing radiation is more prevalent in some donors than others. This is evident from the ability of the classifier to distinguish between sham irradiated and irradiated cells in different donors. Higher sensitivities and specificities indicate a larger change in spectral profile following ionizing radiation, while lower sensitivities and specificities indicate a lack of change in the spectral profile of sham irradiated and irradiated cells (see Table 2). While there is large inter individual variation in the response to ionizing radiation measured by both the γ-H2AX assay and Raman spectral measurements, there is an increase in the band areas that were found to be significantly different from

the control which matched that of the γ-H2AX assay. In both γ-H2AX and Raman spectral measurements a dose response was observed. The correlation between the band areas and the γ-H2AX MFI is shown in Figure 4 B).

Figure 5 A shows the frequency distribution of the γ-H2AX fluorescence measurements with dose for all 20 donors. It demonstrates the frequency of which a measurement of γ-H2AX was measured within a particular range of γ-H2AX MFI for all 20 donors both sham irradiated and irradiated. The black curve represents the probability distribution function and the vertical line represents the mean γ-H2AX fluorescence for each dose. The probability distribution function describes the likelihood of a random measurement to be within a particular interval and the peak of the probability density function is the interval that represents the most likely outcome of any given measurement. The distribution shows an increase in γ-H2AX fluorescence following ionizing radiation as the probability distribution shifts to higher γ-H2AX MFI with the frequency of low levels of γ-H2AX MFI is decreasing and the frequency of higher levels of γ-H2AX MFI is increasing. Large inter-individual variability was observed in the baseline levels of γ-H2AX fluorescence and can be seen from this plot as the frequencies of γ-H2AX MFI span a large range in all doses and overlap between doses. Similarly to the γ-H2AX fluorescence measurements, Figure 5 B shows the frequency distribution of the total area of the regions of the spectrum with higher intensities than the sham in terms of dose. Although the distributions overlap considerably, a positive correlation to γ-H2AX MFI was observed with the total area of the regions that were significantly higher than the control (see Figure 4 B). A shift in the probability distribution function towards higher band areas was observed following ionizing radiation with a decrease in the frequency of lower band areas and an increase in the frequency of higher band areas. The increase in area of these bands is a result of the increase in the intensities observed in the bands at 720-850cm^{-1} associated with the vibrations occurring from the backbones and nucleic acid bases of DNA and RNA and 1640-1660cm^{-1} associated with proteins and lipids. The changes in the distribution of the total area of these bands following ionizing radiation were found to be significantly different in the sham spectra versus the irradiated spectra, with a significance level of $p<0.001$. The significance testing reveals that Raman spectroscopy can detect changes in the spectroscopic finger

print of cells following ionizing radiation in a normal population at 1 hour after exposure to ionizing radiation but as the distributions overlap considerably classification of individual responses becomes more difficult.

5. Discussion

The use of the γ-H2AX assay for dosimetry measurements has been shown previously by *(9)* to have high levels of inter-individual variation, while a dose response following ionizing radiation was observed. In this study, high levels of inter-individual baseline variation has been observed within a cohort of 20 donor lymphocytes and when samples were normalized to their controls a dose response was observed and was found to be statistically significantly. Raman spectroscopy has been shown to be capable of detecting changes in spectral profiles of irradiated lymphocytes compared to sham irradiated lymphocytes at doses as low as 0.05Gy. Unlike the γ-H2AX assay, however, the detection of changes following ionizing radiation are not limited to a single molecule in Raman spectroscopy. Instead Raman spectroscopy provides a cellular biochemical fingerprint containing signatures of nucleic acids, proteins, lipids and fatty acids. The changes in spectral profiles are highly variable from individual to individual matching that of the γ-H2AX inter-individual variability. Large variability in the change in spectral bands associated with nucleic acids (in the region of 720-850cm^{-1}), proteins and lipids (1200-1350cm^{-1}) was observed from individual to individual. The variability in the change in these bands may be due to the variation in age, gender, lifestyle, eating habits and genetic predisposition. PCA-LDA showed poor classification performance when all donors were classified and tested simultaneously, using a leave-one-donor-out cross-validation. Significance testing revealed that there were several regions of the spectrum where the intensities of the spectra of irradiated cells were either significantly higher or lower than that of the control cells. Similarly to the variation observed in the baseline levels of the γ-H2AX assay the areas under these regions overlap considerably between doses making uni-variate classification for the purpose of dosimetry difficult. However, changes to distribution of the area under these regions may provide an alternative method of dosimetry.

Analysis of intensity changes in spectral data with dose

The changes in the intensities of the regions that were observed to differ from the controls following ionizing radiation indicate variation in the spectral information from nucleic acids, lipids and proteins. Increases were observed in the band intensities associated with DNA, RNA, lipids and proteins. This suggests that Raman spectroscopy measures an increase in the level of RNA (band at 750-825cm^{-1}) and thus an increase in transcription and gene expression following ionizing radiation. This is in contrast to that of the γ-H2AX measurements which measures only the phosphorylation of H2AX as a result of ATM activation. The changes in spectral profiles also contain signatures of damage and cellular responses from not only double strand breaks but single strand breaks and other lesion types as the variation in vibrational modes are not limited to alterations in the O-P-O stretching of the DNA backbone. Changes were observed in regions of the spectrum which have been associated with double strand breaks of the DNA *(41)*. Bands around 1110 cm^{-1}, 1160 cm^{-1} and 1190 cm^{-1} were significantly altered after irradiation relative to the sham and are as a result of cleavage of the DNA phosphate backbone at either at the 3' end of one DNA strand and the 5' prime end the other strand or at the 5' end on both strands of the DNA. Some of these changes in spectral profiles are consistent with those observed elsewhere *(42)* after high doses of ionizing radiation.

For a more robust analysis, there is need for larger studies with Raman spectroscopy coupled with parallel reference measurements of DNA damage, repair, cell viability and other high content data. Inclusion of additional data on the individual such as age, gender, ethnicity, lifestyle and health status in modeling of biological data at low doses might also account for the high level of inter-individual variability at low doses. These approaches may in the future provide further insight into the spectral changes following ionizing radiation and will aid in the development of multivariate models.

6. Conclusion

The present study demonstrates the capability of Raman spectroscopy to detect changes in spectral profiles following low dose ionizing radiation in a cohort of 20 donor lymphocytes as little as 1 hour after exposure to ionizing radiation. This is the first report where Raman spectroscopy has been shown to be capable of classifying control samples against irradiated samples with doses as low as 0.05Gy in individuals.

7. Acknowledgments

The authors would like to express sincere thanks to Laura Shields, Chris Walker and Padraic Crean (SLROC) for their generous co-operation. This work was financially supported by the EU FP7 Network of Excellence DoReMi (Grant Number 249689).

8. References

1. Deschavanne PJ, Fertil B. A Review of Human Cell Radiosensitivity in Vitro. Int J Radiat Oncol *Biology*Physics. 1996;34(I):251–66.

2. Marples B, Collis SJ. Low-dose hyper-radiosensitivity: past, present, and future. Int J Radiat Oncol Biol Phys. 2008 Apr 1;70(5):1310–8.

3. Mothersill C, Seymoura CB, Joiner MC. Low-Dose between Relationship Hypersensitivity and the Bystander Effect. Radiat Res. 2002;157(5):526–32.

4. Nasonova E a, Shmakova NL, Komova O V, Mel'nikova L a, Fadeeva T a, Krasavin E a, et al. Cytogenetic effects of low-dose radiation with different LET in human peripheral blood lymphocytes. Radiat Environ Biophys. 2006 Nov;45(4):307–12.

5. Hoeijmakers JHJ. Genome maintenance mechanisms for preventing cancer. 2001;366–74.

6. Jeggo P, Lavin MF. Cellular radiosensitivity: how much better do we understand it? Int J Radiat Biol. 2009 Dec;85(12):1061–81.

7. Burma S, Chen BP, Murphy M, Kurimasa a, Chen DJ. ATM phosphorylates histone H2AX in response to DNA double-strand breaks. J Biol Chem. 2001 Nov 9;276(45):42462–7.

8. Kinner A, Wu W, Staudt C, Iliakis G. Gamma-H2AX in recognition and signaling of DNA double-strand breaks in the context of chromatin. Nucleic Acids Res. 2008 Oct;36(17):5678–94.

9. Horn S, Barnard S, Brady D, Prise KM, Rothkamm K. Combined analysis of gamma-H2AX/53BP1 foci and caspase activation in lymphocyte subsets detects recent and more remote radiation exposures. Radiat Res. 2013 Dec;180(6):603–9.

10. Crow P, Barrass B, Kendall C, Hart-Prieto M, Wright M, Persad R, et al. The use of Raman spectroscopy to differentiate between different prostatic adenocarcinoma cell lines. Br J Cancer. 2005 Jun 20;92(12):2166–70.

11. Krafft C, Steiner G, Beleites C, Salzer R. Disease recognition by infrared and Raman spectroscopy. J Biophotonics. 2009 Feb;2(1-2):13–28.

12. Lyng FM, Faoláin EO, Conroy J, Meade a D, Knief P, Duffy B, et al. Vibrational spectroscopy for cervical cancer pathology, from biochemical analysis to diagnostic tool. Exp Mol Pathol. 2007 Apr;82(2):121–9.

13. Matthews Q, Jirasek a, Lum JJ, Brolo a G. Biochemical signatures of in vitro radiation response in human lung, breast and prostate tumour cells observed with Raman spectroscopy. Phys Med Biol. 2011 Nov 7;56(21):6839–55.

14. Meade AD, Clarke C, Byrne HJ, Lyng FM. Fourier transform infrared microspectroscopy and multivariate methods for radiobiological dosimetry. Radiat Res. 2010 Feb;173(2):225–37.

15. Das K, Stone N, Kendall C, Fowler C, Christie-Brown J. Raman spectroscopy of parathyroid tissue pathology. Lasers Med Sci. 2006 Dec;21(4):192–7.

16. Chan JW, Taylor DS, Zwerdling T, Lane SM, Ihara K, Huser T. Micro-Raman spectroscopy detects individual neoplastic and normal hematopoietic cells. Biophys J. 2006 Jan 15;90(2):648–56.

17. Pully V V., Lenferink a. TM, Otto C. Time-lapse Raman imaging of single live lymphocytes. J Raman Spectrosc. 2011 Feb 15;42(2):167–73.

18. Mannie MD, McConnell TJ, Xie C, Li Y-Q. Activation-dependent phases of T cells distinguished by use of optical tweezers and near infrared Raman spectroscopy. J Immunol Methods. 2005 Feb;297(1-2):53–60.

19. Takai Y, Masuko T, Takeuchi H. Lipid structure of cytotoxic granules in living human killer T lymphocytes studied by Raman microspectroscopy. Biochim Biophys Acta. 1997 Apr 17;1335(1-2):199–208.

20. Chan JW, Taylor DS, Zwerdling T, Lane SM, Ihara K, Huser T. Micro-Raman spectroscopy detects individual neoplastic and normal hematopoietic cells. Biophys J. Elsevier; 2006 Jan 15;90(2):648–56.

21. Lakshmi R., Kartha VB, Murali Krishna C, R Solomon JG, Ullas G, Uma Devi P. Tissue Raman spectroscopy for the study of radiation damage: brain irradiation of mice. Radiat Res. 2002 Feb;157(2):175–82.

22. Krafft C, Neudert L, Simat T, Salzer R. Near infrared Raman spectra of human brain lipids. Spectrochim Acta A Mol Biomol Spectrosc. 2005 May;61(7):1529–35.

23. Ó Faoláin E, Hunter MB, Byrne JM, Kelehan P, McNamara M, Byrne HJ, et al. A study examining the effects of tissue processing on human tissue sections using vibrational spectroscopy. Vib Spectrosc. 2005 Jul;38(1-2):121–7.

24. Stone N, Kendall C, Smith J, Crow P, Barr H. Raman spectroscopy for identification of epithelial cancers. Faraday Discuss. 2004;126:141.

25. Farquharson S, Shende C, Inscore FE, Maksymiuk P, Gift A. Analysis of 5-fluorouracil in saliva using surface-enhanced Raman spectroscopy. J Raman Spectrosc. 2005 Mar;36(3):208–12.

26. Ruiz-Chica AJ, Medina MA, Sanchez-Jimenez F, Ramirez FJ. Characterization by Raman spectroscopy of conformational changes on guanine- cytosine and adenine-thymine

oligonucleotides induced by aminooxy analogues of spermidine. J Raman Spectrosc. 2004;35:93–100.

27. Notingher I, Green C, Dyer C, Perkins E, Hopkins N, Lindsay C, et al. Discrimination between ricin and sulphur mustard toxicity in vitro using Raman spectroscopy. J R Soc Interface. 2004 Nov 22;1(1):79–90.

28. Gniadecka M, Wulf HC, Mortensen NN, Nielsen OF, Christensen DH. Diagnosis of basal cell carcinoma by Raman spectroscopy., 28: 125–129. J Raman Spectrosc. 1997;28:125–9.

29. Lau DP, Huang Z, Lui H, Man CS, Berean K, Morrison MD, et al. Raman spectroscopy for optical diagnosis in normal and cancerous tissue of the nasopharynx-preliminary findings. Lasers Surg Med. 2003 Jan;32(3):210–4.

30. Shaw RA, Mantsch HH. Vibrational biospectroscopy: from plants to animals to humans. A historical perspective. J Mol Struct. 1999 May;480-481:1–13.

31. Malini R, Venkatakrishna K, Kurien J, Pai KM, Rao L, Kartha VB, et al. Discrimination of Normal , Inflammatory , Premalignant , and Malignant Oral Tissue: A Raman Spectroscopy Study. 2006;81:179–93.

32. Seballos L, Zhang JZ, Sutphen R. Surface-enhanced Raman scattering detection of lysophosphatidic acid. Anal Bioanal Chem. 2005 Nov;383(5):763–7.

33. Cheng W-T, Liu M-T, Liu H-N, Lin S-Y. Micro-Raman spectroscopy used to identify and grade human skin pilomatrixoma. Microsc Res Tech. 2005 Oct;68(2):75–9.

34. Dukor RK. Biomedical Applications in Handbook of Vibrational Spectroscopy. 2002.

35. Kolijenovic S, Scut TB, Vincent A, Kros JM, Puppels GJ. Detection of Meningioma in Dura Mater by Raman Spectroscopy. 2005;77(24):7958–65.

36. Kaminaka S, Ito T, Yamazaki H, Kohda E, Hamaguchi H. Near-infrared multichannel Raman spectroscopy toward real-time in vivo cancer diagnosis. J Raman Spectrosc. 2002 Jul;33(7):498–502.

537 *37*. Shetty G, Kendall C, Shepherd N, Stone N, Barr H. Raman spectroscopy: elucidation of
538 biochemical changes in carcinogenesis of oesophagus. Br J Cancer. 2006 May
539 22;94(10):1460–4.

540 *38*. Movasaghi Z, Rehman S, Rehman IU. Raman Spectroscopy of Biological Tissues. Appl
541 Spectrosc Rev. 2007 Sep;42(5):493–541.

542 *39*. Binoy J, Abraham JP, Joe IH, Jayakumar VS, Pettit GR, Nielsen OF. NIR-FT Raman and FT-
543 IR spectral studies andab initio calculations of the anti-cancer drug combretastatin-A4. J
544 Raman Spectrosc. 2004 Nov;35(11):939–46.

545 *40*. Matthews Q, Jirasek A, Lum J, Duan X, Brolo AG. Variability in Raman spectra of single
546 human tumor cells cultured in vitro: correlation with cell cycle and culture confluency. Appl
547 Spectrosc. 2010 Aug;64(8):871–87.

548 *41*. Lipiec E, Sekine R, Bielecki J, Kwiatek WM, Wood BR. Molecular characterization of DNA
549 double strand breaks with tip-enhanced Raman scattering. Angew Chem Int Ed Engl. 2014 Jan
550 3;53(1):169–72.

551 *42*. Matthews Q, Brolo A, Lum J, Duan X, Jirasek a. Raman spectroscopy of single human tumour
552 cells exposed to ionizing radiation in vitro. Phys Med Biol. 2011 Jan 7;56(1):19–38.

553

554 **9.** Table of figures

10. List of tables

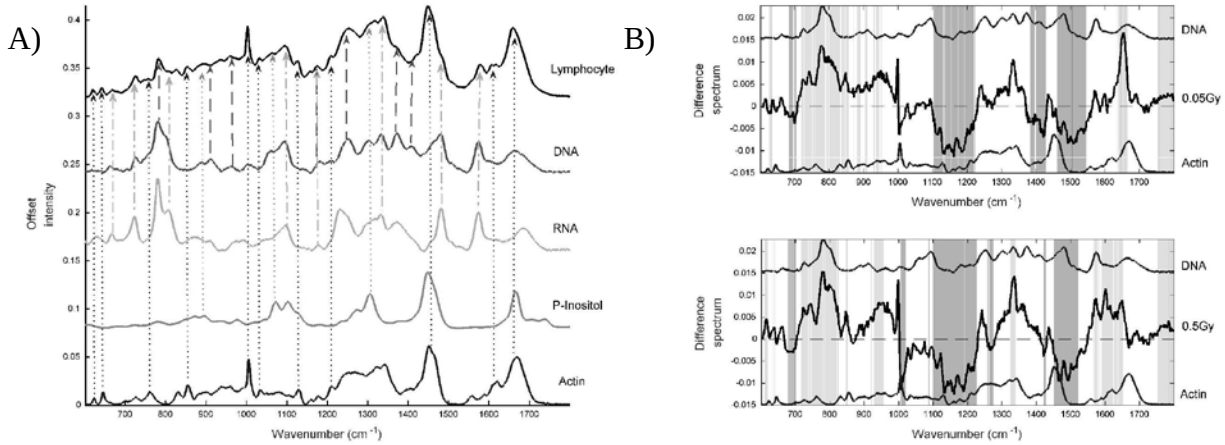

Figure 1: A) The mean of all 20 donors sham-irradiated spectra along with spectra of DNA, RNA, phosphatidyl-inositol (a typical phospho-lipid) and actin (a typical protein). Guides are included to link some modes of vibration in component spectra to modes of vibration in lymphocytes. Pure DNA, RNA, phosphatidyl-inositol and actin were purchased from Sigma-Aldrich and used without further preparation.

B) The difference spectra between sham irradiated and irradiated spectra (0.05Gy and 0.05Gy) along with spectra of DNA and actin. Shaded regions of the spectra represent where the spectrum of irradiated samples were found to be significantly higher (light shading) or significantly lower (darker shading) than the sham irradiated samples.

595 **Table 1:** Raman band assignments for some typical vibrations associated with biological specimens

596

Frequency (cm^{-1})	**Assignment**	**Frequency (cm^{-1})**	**Assignment**
623	C-C twisting mode phenylalanine.	1127	C-N, C-C stretching (protein and lipid)
645	Tryosine		
666	Guanine, Thymine ring breathing	1175	Cytosine, Guanine, C-H bending
723	Adenine		tyrosine (proteins)
749	Tryptophan	1210	Tyrosine,
780	Cytosine, Uracil,		Phenylalanine
	Thymine (Ring	1230-1295	Amide III
	breathing)	1332	C_3-C_3 stretch, C_5-O_5
807	O-P-O backbone (DNA/RNA)		stretch and CH_α in plane bending,
855	Tyrosine		Guanine
941	Skeletal modes (polysaccharides)	1370	Thymine, Adenine, Guanine
1003	Phenylalanine	1430-1460	C-H_2 deformation
1032	C-H bending	1485	Amide II, Guanine,
1064	Phenylalanine ,C-C		Adenine
	stretch of lipids	1552	Tryptophan
1085	C-O stretching	1575	Guanine, Adenine
1095	PO_2^- from nucleic acids	1614/15	C=C (protein) Tyrosine, Tryptophan,
		1650-1680	Amide I, C=C stretching (proteins)

597

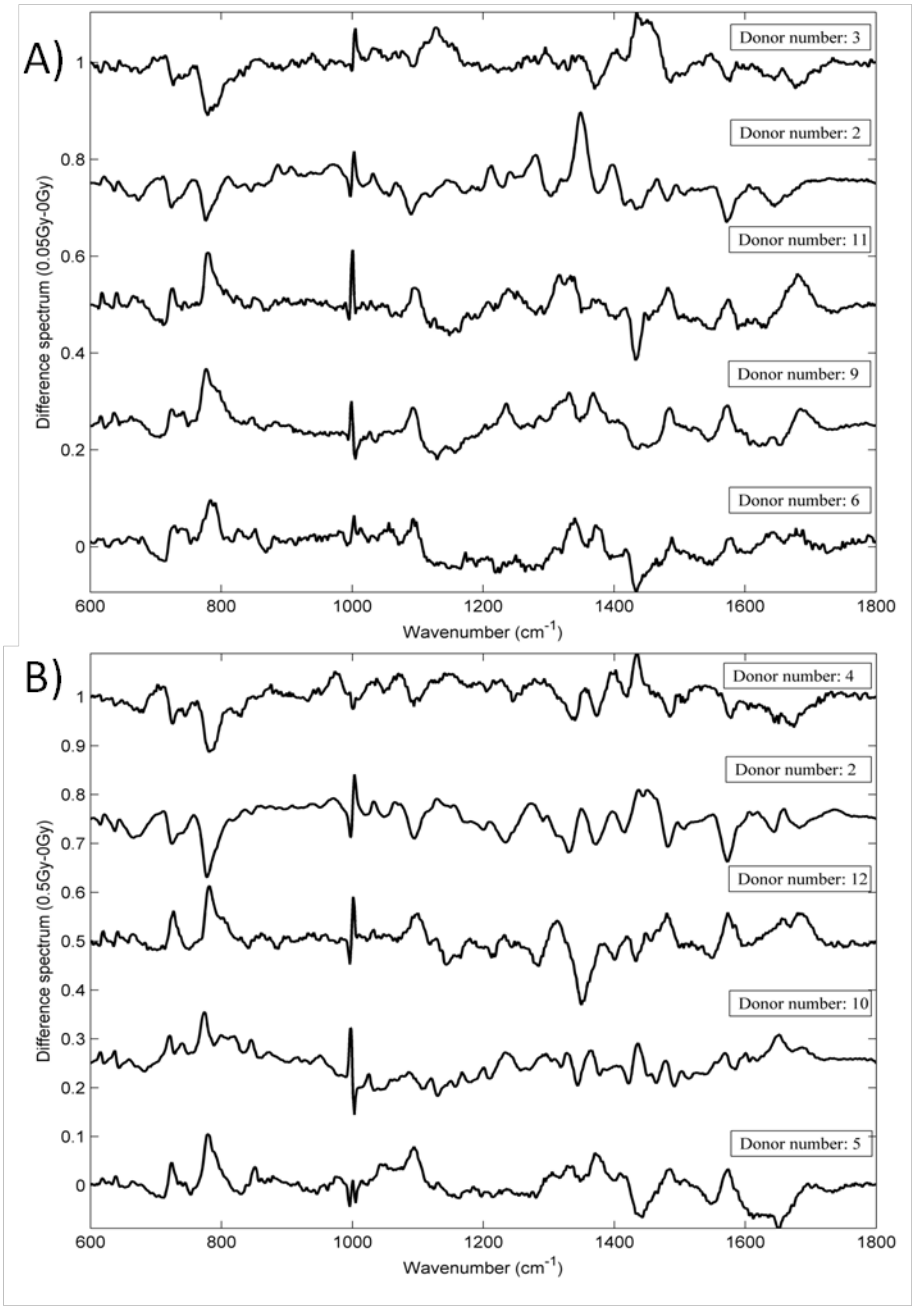

598

599 **Figure 2**: A) Difference spectra of 0.05Gy and 0Gy for 5 donor's spectra and B) Difference spectra of 0.5Gy and 0Gy for 5

600 donor's spectra.

601

602

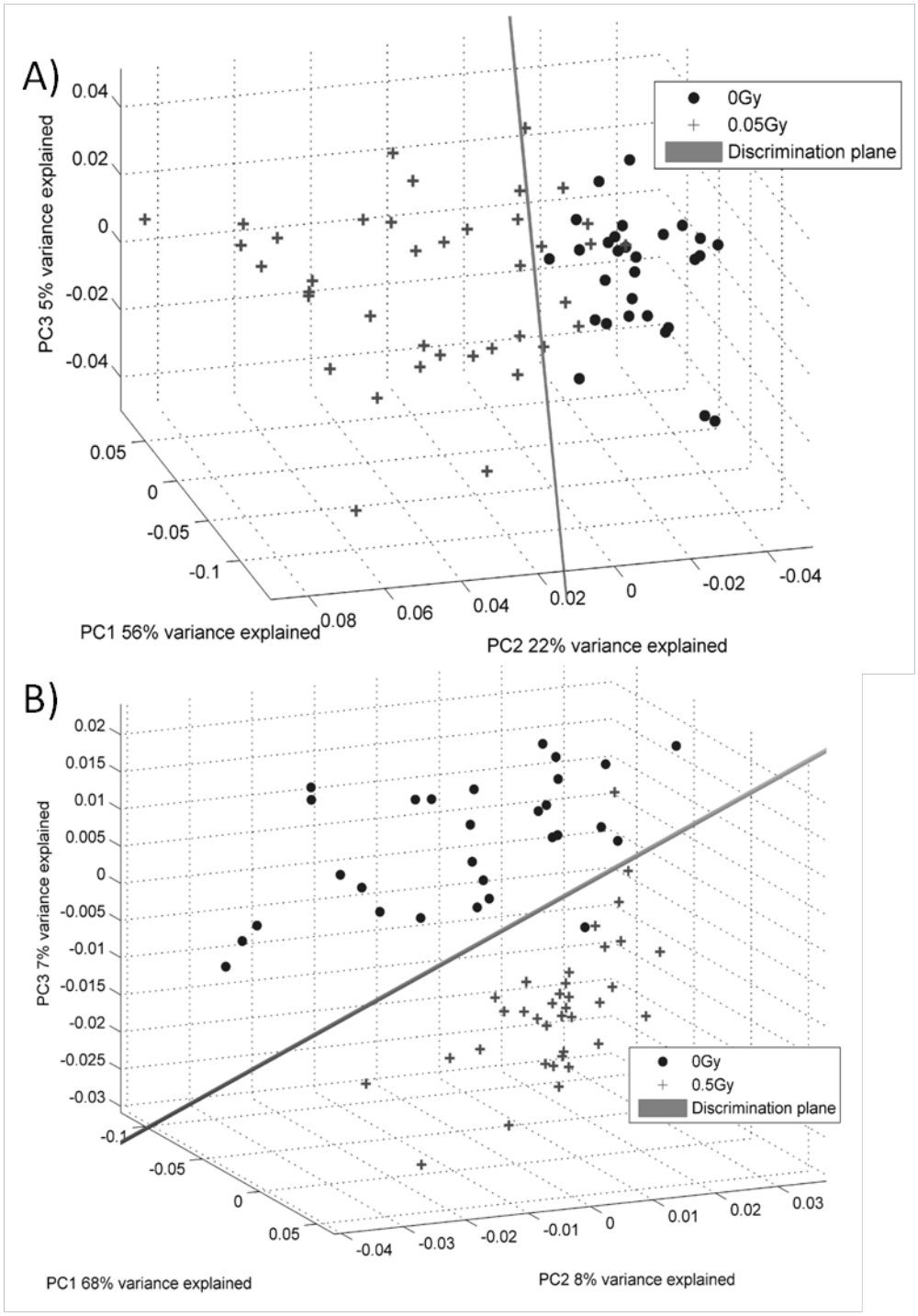

Figure 3: The scatter plots of PCA scores of 0Gy and 0.05Gy (A), and 0Gy and 0.5Gy (B) spectra of a single healthy donor and for the first three principal components. The grey line represents the plane of discrimination determined by LDA.

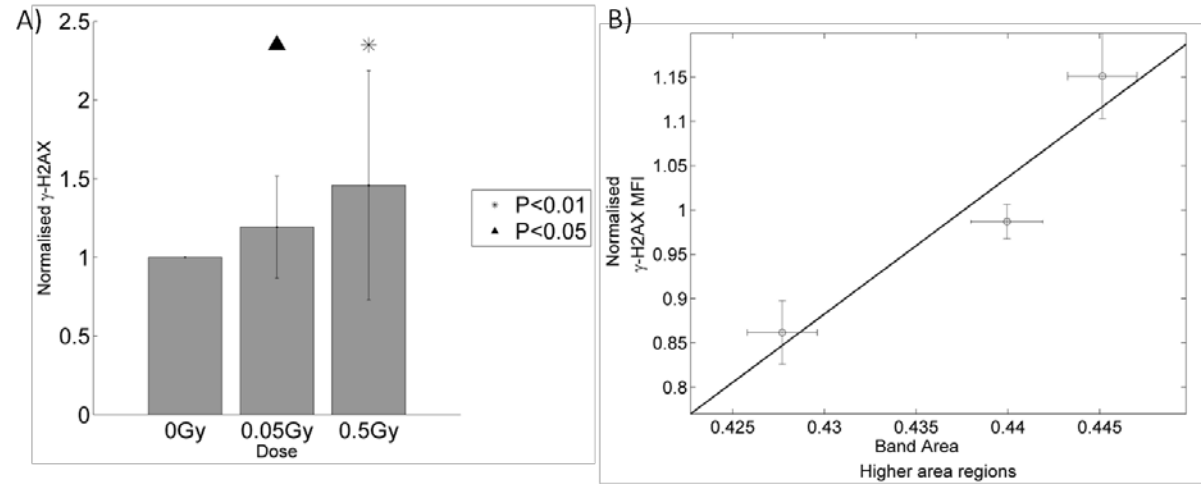

607

608 **Figure 4**: A) Normalised γ-H2AX fluorescence with respect to dose for all donors. Significance testing was performed using
609 a two tailed paired t-test. B) Normalised γ-H2AX MFI with respect to the total area of the bands of the spectrum that were
610 found to be significantly higher than the sham. Error bars indicate the standard error.

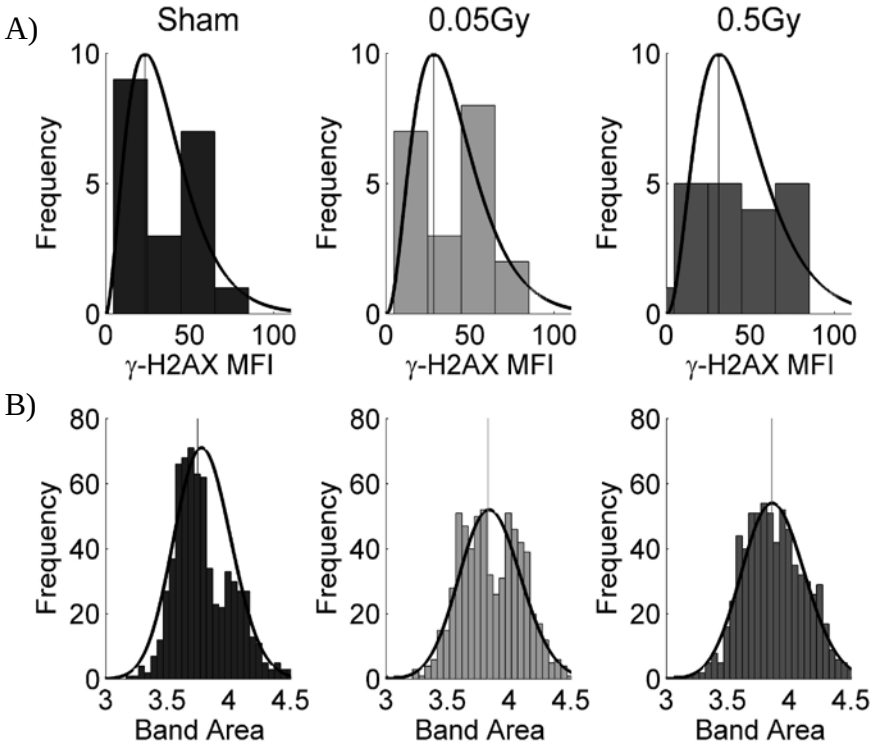

611

612 **Figure 5**:A) The frequency distribution (the number of measurements that fell within an interval of MFI) of γ-H2AX
613 fluorescence for sham irradiated (0Gy) and irradiated cells (0.05Gy and 0.5Gy). The black curve represents the probability
614 density function and the vertical black line represents the maximum probability of the probability density function. B) The
615 frequency distribution of the area of the region of the spectrum that was found to be significantly higher following ionizing
616 radiation.

617

Table 2: Sensitivities and specificities for the classifications of 0Gy versus 0.05Gy, 0Gy versus 0.5Gy and 0.05Gy versus 0.5Gy spectra for each donors spectra. Donors are ordered in terms of decreasing sensitivities, larger sensitivities and specificities indicate larger changes in spectral profiles following ionizing radiation.

Donor no.	0.05Gy		Donor no.	0.5Gy		Donor no.	0.05Gy v 0.5Gy	
	Sensitivity	Specificity		Sensitivity	Specificity		Sensitivity	Specificity
10	1.00	1.00	2	1.00	1.00	1	1.00	1.00
11	1.00	0.96	8	1.00	1.00	2	1.00	1.00
15	1.00	0.94	10	1.00	1.00	15	1.00	1.00
9	0.97	0.92	20	1.00	1.00	7	1.00	1.00
2	0.96	1.00	1	1.00	0.97	8	1.00	1.00
8	0.95	0.94	15	1.00	0.90	5	1.00	0.93
20	0.93	1.00	12	0.98	0.96	19	1.00	0.88
7	0.93	0.86	19	0.97	0.92	12	0.97	0.94
19	0.92	0.94	5	0.97	0.97	13	0.97	0.97
18	0.91	0.91	7	0.96	0.86	10	0.97	0.90
14	0.91	1.00	14	0.93	1.00	17	0.97	0.82
3	0.90	0.93	3	0.92	1.00	20	0.96	0.91
12	0.90	0.85	9	0.92	0.89	16	0.91	1.00
1	0.86	0.84	17	0.91	0.83	9	0.90	0.97
13	0.82	0.94	16	0.86	0.97	6	0.90	0.82
5	0.81	1.00	6	0.86	0.93	18	0.88	1.00
6	0.79	0.89	18	0.84	0.91	3	0.85	0.93
4	0.76	0.80	4	0.82	0.91	14	0.82	0.92
16	0.71	0.82	13	0.81	0.89	11	0.81	0.73
17	0.67	0.82	11	0.78	0.85	4	0.79	0.79
Mean	0.90	0.92	Mean	0.93	0.94	Mean	0.94	0.93